Production of excited H atoms at the C 1*s* edge of the methane molecule studied by VUV-photon–photoion and metastable-fragment–photoion coincidence experiments

A. Kivimäki,[1,*] J. Álvarez-Ruiz,[2] R. Sergo,[3] and R. Richter[3]

[1]*Consiglio Nazionale delle Ricerche - Istituto Officina dei Materiali, Laboratorio TASC, 34149 Trieste, Italy*

[2]*Instituto de Fusión Nuclear, Universidad Politécnica de Madrid, José Gutiérrez Abascal 2, 28006 Madrid, Spain*

[3]*Elettra–Sincrotrone Trieste, Area Science Park, 34149 Trieste, Italy*

(Received 21 June 2013; published 9 October 2013)

Coincidences between neutral particles and photoions have been measured at the C 1*s* edge of the CH_4 molecule. These neutral particles are either vacuum ultraviolet (VUV) photons or metastable fragments and their contributions can be separated temporally. Observed VUV-photon–photoion coincidences were mostly triggered by Lyman emission in excited H atoms. Two metastable fragment-photoion channels were observed and assigned to H^*-H^+ and H^*-CH_n^+ ($n = 0$–3) coincidences, where H^* signifies a metastable H atom. The coincidence yields as a function of photon energy revealed all the core excitations, but were particularly enhanced just above the C 1*s* ionization threshold and also displayed the vibrational structure related to the core-ionized C $1s^{-1}$ state. The metastable H atoms observed in the present study were produced in highly excited Rydberg states and could be partly field ionized. The approximate kinetic energy distributions of the metastable H^* atoms have been derived from the H^*-H^+ coincidence measurements performed at the C $1s \rightarrow 3p$ and $3d$ resonances as well as just above the C 1*s* threshold.

DOI: 10.1103/PhysRevA.88.043412 PACS number(s): 33.80.Gj, 33.80.Rv, 33.15.Ta, 33.20.Ni

I. INTRODUCTION

Hikosaka *et al.* [1] observed in 2005 that particularly many excited, long-living neutral N atoms were produced in photoionization of the N_2 molecule, when the photon energy was tuned to the vicinity of the N 1*s* ionization potential (IP). The authors attributed the enhanced production of the metastable atoms (N^*) to recapture processes that occur in the context of post-collision interaction (PCI). Just above the N 1*s* threshold a slow photoelectron is overcome by a subsequently emitted, but faster Auger electron. The two electrons can exchange energy and the photoelectron can even be pushed back to the molecule, occupying a Rydberg orbital. An electronic state with two valence holes and an electron in a Rydberg orbital is thus formed; such a state can be denoted as a two-hole one-electron (2h-1e) state or as a $\mathrm{val}^{-2}n\lambda^1$ state, where val indicates a valence orbital and $n\lambda$ gives the principal and orbital quantum numbers of the Rydberg orbital. The dicationic core starts to dissociate into two N^+ ions. The molecular Rydberg electron ends up in a Rydberg orbital of one of the fragment ions, which thus becomes an excited neutral atom. Lifetimes of the Rydberg excited states $\mathrm{val}_1^{-1}nl^1$, which are built around a vacancy in the outermost orbital val_1, are proportional to n^3 and can be in the microsecond range, if the principal quantum number n is sufficiently high ($\approx$15–40). Nitrogen atoms in high-n Rydberg states were efficiently produced also just below the N 1*s* threshold, where the initial excitation promotes an N 1*s* electron to a high-n Rydberg orbital of the molecule [1]. The principal quantum number of the Rydberg electron is not expected to change appreciably during resonant Auger decay of core-excited states and subsequent dissociation. Similarly, metastable fragments have been observed at the Cl 2*p* edge of the HCl molecule [2], at the O 1*s* edge of the H_2O molecule [3], and at the C 1*s* edge of the CO molecule [4], implying that their creation is a general phenomenon in threshold photoionization of molecular inner shells. Measurements above the core ionization thresholds have revealed that metastable fragments were also created at core-valence double excitations and at 1*s* photoionization shake-up thresholds of the N_2 and CO molecules [4,5].

Some atomic states are metastable because their fluorescence decay to lower energy states is dipole forbidden. The hydrogen atom in the 2*s* state, H(2*s*), is an example. In principle, fluorescence decay is allowed from highly excited Rydberg states ($\mathrm{val}_1^{-1}nl^1$), but it becomes less and less probable as n increases. Such states can then be considered metastable if they do not fluoresce within the execution time of a particular experiment. In addition, truly metastable states can be formed as a result of low-energy fluorescence cascades. It is therefore not surprising that fluorescence emission in neutral fragments has been observed at the core edges of many small molecules such as N_2, H_2O, NH_3, CH_4, and CO_2 [6–10]. Fluorescence emission in fragments is usually enhanced at all core excitations of the studied molecules, but the enhancement has been found to be particularly large, when the initial excitation reaches Rydberg orbitals with $n \geqslant 4$ or 5, i.e., in the region close to the core IP [7–10]. Emission has also been found to persist while crossing the core IP, after which it diminishes gradually as a function of photon energy. That behavior has been attributed to recapture processes following core ionization and Auger decay [10,11]. All in all, low-energy fluorescence emission after core excitation and ionization in small molecules can be explained using the same mechanisms as the production of metastable fragments.

In experiments aimed at the detection of neutral particles, charged particles can be avoided by a suitable choice of potentials in the apparatus. However, special experimental arrangements are usually necessary to study metastable atom formation because microchannel plate (MCP) detectors, which have been used in the above-mentioned experiments [1–5],

*Corresponding author: kivimaki@iom.cnr.it

also detect VUV and soft x-ray photons. Hikosaka *et al.* [1] measured the yield of N^* atoms in coincidence with N^+ ions at the N 1*s* edge of N_2 using two MCP detectors facing each other. In Refs. [2–5], a special filling mode of the SPring-8 storage ring was exploited in such a way that the signal observed around the arrival times of synchrotron light bunches was vetoed, avoiding the detection of fluorescence emission in the excited fragments with lifetimes in the low nanosecond range. The signal during the remaining time was assumed to arise from metastable atoms, allowing one to record clean yields of metastable atoms. In a study of H_2O, Harries *et al.* [3] coupled the metastable atom detection with an ion time-of-flight (TOF) spectrometer. They observed the yields of H^* in coincidence with different ions, thus obtaining more detailed knowledge of dissociation channels that produce metastable fragments.

Methane, CH_4, is the simplest saturated hydrocarbon. Its electron configuration in the ground state (T_d symmetry) is $1a_1^2 2a_1^2 1t_2^6$, where $1a_1$ is the C 1*s* orbital, and $2a_1$ and $1t_2$ are the C-H bonding valence orbitals. Methane also has two unoccupied antibonding valence orbitals $3a_1$ and $2t_2$. It appears, however, that atomiclike Rydberg orbitals $3sa_1, 3pt_2, 3dt_2, \ldots$ are much more important for electronic transitions in methane than the antibonding orbitals. For instance, the valence absorption spectrum of CH_4 can be interpreted as transitions to Rydberg orbitals [12,13]. The core excitation spectrum below the C 1*s* IP is also commonly attributed to C $1s \rightarrow$ Rydberg transitions, while the empty valence orbitals may induce a small amount of valence character in some core-excited states [14,15]. Photodissociation of CH_4 into ionic fragments has been studied extensively in the valence and inner-shell regions (see, e.g., [16], and references therein). Metastable molecular fragments have been observed upon 60 eV electron impact on methane [17], while the creation of excited H atoms is a common phenomenon in valence and core photoionization of methane (see, e.g., [9,18]). In the present paper, we study the production of neutral fragments at the C 1*s* edge of CH_4 by exploiting VUV-photon–photoion and metastable-fragment–photoion coincidence measurements. The metastable-fragment–photoion coincidences are found to be strongly enhanced at the C 1*s* threshold of CH_4.

II. EXPERIMENT

The experiments were carried out at the Gas Phase Photoemission beamline [19] at the Elettra synchrotron radiation facility in Trieste (Italy). The beamline receives radiation from an undulator in the photon energy range of about 14–900 eV and uses a spherical grating monochromator to provide intense and highly monochromatic light in a chosen experimental station. The electron storage ring operated in the usual multibunch mode with 2 ns separation between electron bunches.

A scheme of the experimental setup is shown in Fig. 1. Briefly, it consists of a time-of-flight spectrometer (with the drift tube length of 105 mm) to separate ions based on their mass to charge ratio and an MCP detector to detect neutral particles. The devices were installed along the electric vector of the linearly polarized incident light. The general setup was already presented in [10], hence only the changes to it are discussed here. First, the gas inlet system via a

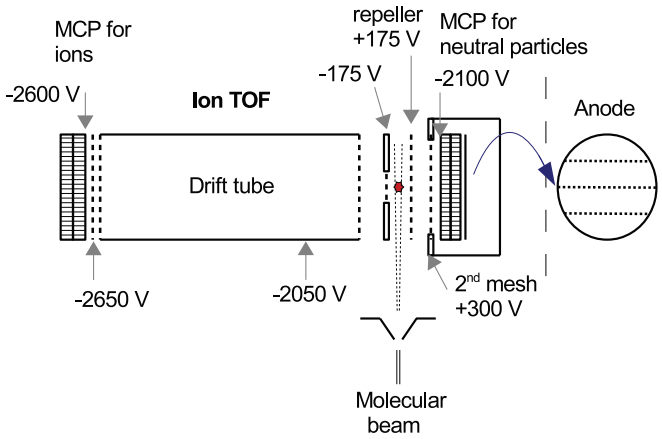

FIG. 1. (Color online) A scheme of the experimental setup used to measure coincidences between neutral particles and photoions. The front view of the four-sectioned anode is shown on the right side. Typical potentials used at different surfaces are also given. The distance between the two meshes at ±175 V was 11 mm, the distance between the repeller mesh (at +175 V) and the second mesh (at +300 V) was 7 mm, and the distance between the second mesh and the front of the MCP was 4.5 mm.

hypodermic needle was replaced by a supersonic molecular beam that advanced from bottom to top and crossed the photon beam perpendicularly. Pressure of the CH_4 gas in the gas inlet system (i.e., before expansion into the vacuum chamber) was about 0.17 bar, while pressure in the experimental chamber was 9×10^{-7} mbar during the measurements. Second, the microchannel plate detector used for VUV-photon and metastable particle detection was changed. A standard MCP can detect VUV photons with wavelengths shorter than ∼150 nm and metastable atoms with a comparable amount of internal energy, i.e., above ∼8.3 eV. Neutral atoms can also be detected with MCPs by virtue of their kinetic energy, but then the threshold is hundreds of eVs [20]. The new MCP detector was equipped with a specifically constructed anode, consisting of four horizontal sections. Signals could be obtained independently from each section of the anode, while capacitive coupling allowed a free choice of the polarization of the detector. The intensity of the incident photon beam was monitored with a Si photodiode located at the exit of the experimental chamber. The photon energy scale was calibrated according to the C $1s \rightarrow 3pt_2$ excitation at 288.00 eV [21]. The width of the incident photon band was about 0.1 eV in most neutral particle-photoion coincidence measurements.

The potentials on the meshes around the interaction region, which is marked by a star in Fig. 1, and on the front side of the neutral-particle detector were such that cations, anions, and electrons created in the interaction region could not reach the detector. We still needed to separate the start signals originating from VUV photons and from metastable fragments because both can be detected by an MCP. This was done by recording them in coincidence with positive ions. We used the signals from the four-sectioned anode of the neutral-particle detector as start signals for time-resolved coincidence measurements, while stop signals were taken from the MCP detector of the ion TOF spectrometer. These signals were fed in the time-to-digital converter system (ATMD-GPX [22]). VUV photons provide

prompt start signals, as fluorescence lifetimes are generally short. Hence VUV-photon–photoion coincidence spectra consist of well-defined peaks. Metastable fragments are slower, providing delayed start signals, and are likely to have wide kinetic energy distributions. Metastable-fragment–photoion coincidences are therefore expected to form broad structures at shorter relative arrival times than those initiated by VUV photons. To be able to detect more clearly such coincidences, we delayed the stop (photoion) signals electronically by 3.0 μs. The neutral-particle–photoion coincidence spectra shown in this paper display the number of coincidences binned in 4 ns intervals.

We observed contamination signals in VUV-photon–photoion coincidence spectra during previous measurements [10]. The source of contamination could not be identified at that time, but during the present experiments we realized that those coincidences were caused by electrons that were created when photoions hit the mesh in front of the MCP detector of the ion TOF spectrometer or the MCP itself (see Fig. 1). As shown below, that contamination signal could be reduced drastically with the use of the four-sectioned anode.

III. RESULTS AND DISCUSSION

A. Interpretation of the coincidence spectra

Figure 2 shows the neutral-particle–photoion coincidence spectra of CH_4 measured at the photon energy of 288.0 eV, which corresponds to the maximum of the C 1$s \rightarrow 3pt_2$ excitation. The upper spectrum was obtained when the whole surface of the neutral-particle detector was used, while in the lower spectrum only the two outermost sections of the anode were connected to the electronics modules. The spectra have been normalized to the same height at the sharp peak around 3400 ns, after which one of the spectra was shifted upwards for clarity. Because of the delay of the ion signal by 3000 ns, the zero of the real time scale is at 3000 ns. We can attribute the observed structures to three different types of start signals.

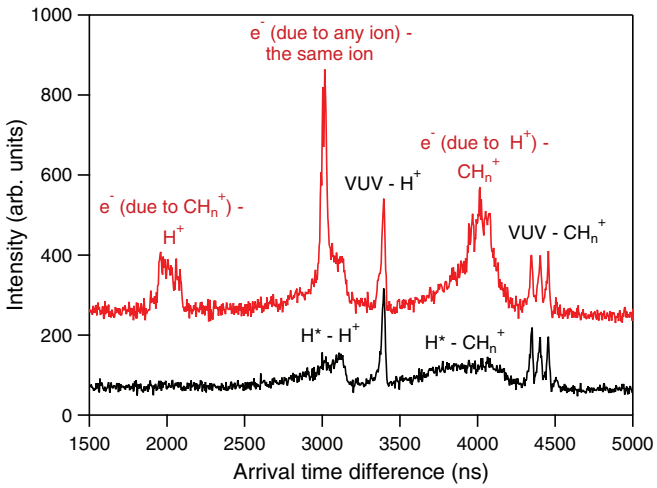

FIG. 2. (Color online) Neutral-particle–photoion coincidence spectra of CH_4 measured at the photon energy of 288.0 eV (C 1$s \rightarrow 3pt_2$ excitation). The top spectrum was measured using the whole anode of the neutral-particle MCP detector, while in the bottom spectrum only the two outermost sections of the anode were connected. Different contributions to the coincidence spectrum are labeled (see text for details). The photoion signal has been delayed by 3.0 μs.

(1) VUV photons emitted in the interaction region give rise to sharp coincidence peaks, if molecular dissociation is fast and the lifetime of the VUV emitting state is relatively short. A vast majority of these start signals is expected to arise from Lyman emission due to excited H atoms. Lyman-α emission [H(2p) $\rightarrow$ H(1s) transitions] has been observed at this resonance [9]. As the initial resonant excitation is to the 3p orbital, Lyman-β emission [H(3p) $\rightarrow$ H(1s) transitions] is also expected to be important. The lifetime of the H(3p) state is about 5.4 ns [23]. The three sharp peaks just below 4500 ns in Fig. 2 can be assigned to the VUV-photon–CH_n^+ coincidences, where n = 0–2, while the CH_3^+ ion barely rises above the background at 4500 ns. The peak at 3400 ns is assigned to VUV-photon–H^+ coincidences. It shows a slight asymmetry to the left side in accord with a lifetime in the few nanosecond range; the FWHM of this peak is ~25 ns, but also the kinetic energy distribution of the detected photoion contributes to the observed line shape. The attributions of the peaks agree with the photoelectron-photoion coincidence (PEPICO) measurements that were performed with the same potentials around the interaction region and in the ion TOF spectrometer. A PEPICO spectrum measured just above the C 1s IP revealed a very weak C^{2+} peak but no other dicationic peaks, in agreement with earlier studies [24,25]. The intensity of possible VUV-photon–C^{2+} coincidences did not rise above the detection level in our experiments.

(2) The second contribution is represented by the coincidence peaks at about 2.0, 3.0, and 4.0 μs in the top spectrum of Fig. 2. These peaks practically disappeared when only the two outermost sections of the anode of the neutral-particle detector were used. We attribute them to a contamination signal due to electrons that were created when photoions hit the mesh in front of the ion detector or the front side of the detector itself. Because these two surfaces were at higher negative potentials than the front side of the neutral-particle detector, such electrons could be accelerated backwards along the drift tube, cross the interaction region, and be detected at the neutral-particle detector. It took about 20 ns for electrons to complete that passage. If the same ion that caused electron emission from the mesh or MCP was detected in coincidence with the electron, a coincidence peak arose close to the zero of the time scale (which was at 3000 ns) because that ion was already close to or even in the ion MCP detector. If another ion was detected in coincidence with such an electron, the resulting coincidence peak appeared at a position different from 3000 ns. Our assignment of the electron-photoion coincidence peaks is given in Fig. 2. Note that if a CH_n^+ ion caused electron emission from the mesh or the ion MCP, the H^+ ion from the same dissociation event had already been observed and the coincidence peak appeared before the real zero of the time scale. From another point of view, one could consider that a part of this "electron contamination signal" originated from true photoion-photoion coincidences that were detected in an indirect way.

(3) When only the two outermost sections of the anode were used in the coincidence measurement, two broad features

around 3.0 and 4.0 μs were clearly brought forth (see the bottom spectrum of Fig. 2). We assign them to metastable-fragment–photoion coincidences. Metastable fragments are, of course, slower than VUV photons and their kinetic energies are expected to have wide distributions. This is in agreement with the large widths and positions of these coincidence features. The one at around 3.0 μs corresponded to the arrival of the H^+ ion, while the other feature was due to the detection of a heavier fragment (probably any of CH_n^+, where $n = 0$–3, even though the masses were not resolved). Based on the time difference between the start signals generated by VUV and metastable fragments, the metastable fragment is calculated to be so fast that it could conceivably be only H (see also Sec. III E).

Electron-induced coincidences can be barely seen around 3000 ns in the bottom spectrum of Fig. 2. The flow of electrons from the ion TOF to the neutral-particle detector was thus significant only close to the symmetry axis of the experimental setup. Other neutral-particle–photoion coincidence spectra discussed in this study were measured using the two outermost sections of the neutral-particle MCP detector. Contamination due to electron start signals was found to be of the same magnitude as in the bottom spectrum of Fig. 2. When the spectrometer is operated in the normal PEPICO mode, contamination peaks are almost invisible.

B. Coincidence spectra below the C 1*s* edge

The spectra of Fig. 2 were measured at the C $1s \rightarrow 3pt_2$ excitation. The created core-excited state decays predominantly via spectator Auger transitions, populating mostly $(\mathrm{val})^{-2}3pt_2^1$ states [15,26], where val (=valence) is $1t_2$ or $2a_1$. These singly ionized final states have binding energies higher than 25 eV. According to the PEPICO study of Field and Eland [27], such ionic final states always fragment. The excited electron in the $3p$ orbital in the parent ion can end up in an excited orbital of some fragment during dissociation. If a hydrogen atom in the $3p$ state is created (adiabatic dissociation), it can decay by Lyman-β emission ($3p \rightarrow 1s$ transition) or by Balmer-α emission ($3p \rightarrow 2s$ transition). The branching ratios of these transitions have been calculated to be 88% and 12%, respectively [28]. In the case of Lyman-β emission, a photon at 102.6 nm is emitted, which can be detected by the MCP detector and can lead to an observed coincidence event. All VUV-photon–photoion coincidences observed in the spectrum can be explained by this mechanism. For instance, dissociation $CH_4^+[(\mathrm{val})^{-2}3p^1] \rightarrow H(3p) + H^+ + CH_2$, followed by Lyman-$\beta$ emission in the excited H atom, would bring up the VUV-H^+ coincidence peak (the constituents of CH_2 can naturally appear as smaller fragments as well). If the H($3p$) atom decays by Balmer-α emission, which has been observed at this resonance [9], a metastable H($2s$) atom is formed. As discussed below, H($2s$) states are expected to be depleted because of the electric field in the interaction region. Therefore, in order to explain the observed H^*-photoion coincidences, we need to assume that H atoms are produced in higher Rydberg states after resonant Auger decay. We denote such atoms as H(HR). Their identity will be discussed in more detail in Section III D.

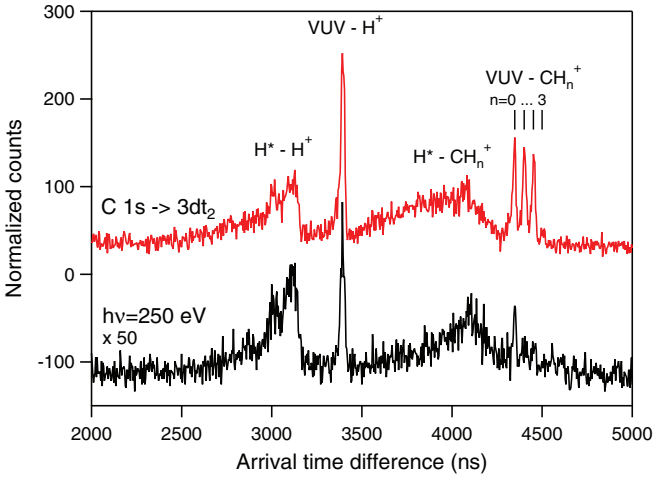

FIG. 3. (Color online) Neutral-particle–photoion coincidence spectra of CH_4 measured at the photon energies of 288.7 eV (C $1s \rightarrow 3dt_2$ excitation) and 250 eV (bottom). The intensity of the bottom spectrum has been multiplied by 50. The photoion signal was delayed by 3.0 μs. The measuring time for each spectrum was 2 h.

Figure 3 shows the VUV photon/H^*-photoion coincidence spectra measured at the photon energies of 250 and 288.7 eV. The former energy can only induce valence ionization processes, while the latter photon energy corresponds to the C $1s \rightarrow 3dt_2$ excitation [15,29]. The coincidence spectrum measured at the C $1s \rightarrow 3dt_2$ resonance is very similar to the spectrum measured at the C $1s \rightarrow 3pt_2$ resonance (the lower spectrum in Fig. 2). The only difference in relative intensities is that the VUV-CH_n^+($n = 0$–3) coincidence peaks appear slightly weaker at the C $1s \rightarrow 3dt_2$ resonance. If adiabatic dissociation occurs after resonant Auger decay from the C $1s^{-1}3dt_2^1$ state, one expects an enhanced production of hydrogen atoms in the $3d$ state. This excited atom can decay via H($3d$) $\rightarrow$ H($2p$) $\rightarrow$ H($1s$) emissions in field-free conditions. The second-step photon emission (Lyman-α) could be detected in our experiment, which should favor the occurrence of VUV-photon–photoion coincidences in the spectrum. We do not observe this in our experiment; in contrast, the coincidence spectrum is similar to the one measured at the C $1s \rightarrow 3pt_2$ excitation, where both VUV-photon–photoion and H^*-photoion coincidences are expected. We attribute this to the fact that in the presence of an electric field the H($3l$) states mix with each other, their degeneracy is removed, and the transition probabilities change [30]. Hydrogen states in the electric field are discussed in more detail in Sec. III D. A neutral-particle–photoion coincidence spectrum was also recorded at the C $1s \rightarrow 3pt_2 + \upsilon_1$ excitation [15,29], where the excitation of the symmetric stretch vibration accompanies the electronic transition. The result (not shown) was similar to the one obtained at the C $1s \rightarrow 3pt_2$ resonance.

Direct valence photoionization also results in neutral-particle–photoion coincidences, as can be seen from the measurement done at the photon energy of 250 eV (lower spectrum of Fig. 3). Note, however, that the normalized intensity of the spectrum at $h\nu = 250$ eV is about 50 times lower than at the C $1s \rightarrow 3dt_2$ excitation. The relative intensities of the coincidence peaks differ in the two spectra. In particular, the

VUV-photon–photoion coincidence peaks are more intense at the resonance energy. This is because resonant Auger decay of the C $1s^{-1}3dt_2^1$ state and subsequent dissociation predominantly produce hydrogen atoms in low-Rydberg states with $n \approx 3$, which emit VUV and visible photons within a few nanoseconds, favoring the VUV-photoion coincidences. (The argument is also valid for the C $1s^{-1}3pt_2^1$ core-excited state.) The H*-CH_n^+ coincidence feature is wider at the C $1s \rightarrow 3dt_2$ excitation than at $h\nu = 250$ eV, which indicates the ejection of slower metastable atoms at the resonance energy.

The production of excited H atoms in valence photoionization of CH_4 has been studied at much lower photon energies and it has been mostly attributed to doubly excited states (see, e.g., [18]). Such states are not populated at the photon energy of 250 eV, but it is likely that excited H atoms are also produced in direct ionization via population of so-called correlation satellite states, which appear in the inner-valence photoelectron spectrum of CH_4 [31]. The most intense of them were attributed to $\mathrm{val}^{-2}2t_2^1$ and $\mathrm{val}^{-2}3a_1^1$ states, which involve the occupation of the antibonding valence orbitals. However, regarding the general importance of Rydberg orbitals in the excited states of methane, the correlation satellite intensity may be mostly due to the population of $\mathrm{val}^{-2}\mathrm{Ryd}^1$ states. Such an attribution would also be in line with the assignment of the C 1s shake-up photoionization spectrum of methane [32]. If $\mathrm{val}^{-2}\mathrm{Ryd}^1$ states are produced in direct valence photoionization, excited H atoms can be created in subsequent dissociation. Similar states are reached after resonant Auger decay, but in direct valence photoionization the n range of Rydberg orbitals populated is more widely spread. If n of the Rydberg orbital in the correlation satellite state is high enough, subsequent dissociation can create metastable H atoms. We suggest that this is the origin of the H*-photoion coincidences observed in our experiments at $h\nu = 250$ eV.

The VUV-photoion coincidences in the same spectrum follow the dissociation of correlation satellite states when lower molecular Rydberg orbitals are populated. The lower Rydberg orbitals are more likely to be populated in photoionization than higher Rydberg orbitals, yet the area of the H*-photoion coincidence features is larger than that of VUV-photoion features at the photon energy of 250 eV. (From a discussion presented in Sec. III D, we estimate that the limit between the low and high Rydberg orbitals in this context may be located at $n \approx 7$.) The detection of metastable atoms by the MCP detector therefore appears to be much more efficient than the detection of Lyman radiation. We cannot estimate the detection efficiencies of VUV photons and metastable atoms because the relative numbers of each type of particles are not known after dissociation. Furthermore, some metastable H atoms were field ionized before reaching the MCP detector (see Sec. III D), and acceleration of resulting protons greatly enhanced their detection efficiency [33].

It is interesting to note that among the VUV-photon–CH_n^+ coincidence peaks, the VUV-photon–C^+ peak is the strongest one after direct valence photoionization. In contrast, C^+ was the second weakest ion after H_2^+ in the partial ion yields measured around the photon energy of 250 eV [16]. In VUV-photon–photoion coincidence measurements, the C^+ ion can appear if C^+ is so highly excited that it itself emits a VUV photon or if C^+ is created together with a VUV-emitting H* atom. The small branching ratio of the C^+ ions at $h\nu = 250$ eV [16] and the "high" intensity of the VUV-photon–C^+ peak imply that the former channel is predominant; the process is surely possible if the created C^+ ion has a vacancy in the 2s subshell [10]. VUV emission from molecular fragments is probably very weak or negligible. VUV-photon–CH^+ and –CH_2^+ coincidence peaks, which were barely visible at 250 eV photon energy, are deduced to arise when VUV emission takes place in H*. In conclusion, if valence ionization is followed by VUV-photon emission, dissociation of CH_4^+ to H* + CH_n^+ ($n = 1$–3) is not particularly likely, but the smallest ionic fragments H^+ and C^+ are favored.

C. Production of H* atoms at the C 1s edge

The yields of H(HR)-H^+ and H(HR)-CH_n^+ coincidences were measured by collecting ions that arrived within the time windows of 2.4–3.2 and 3.45–4.25 μs, respectively. The windows were carefully set not to contain any VUV-photoion coincidence peaks (see Figs. 2 and 3). An equally long window was set up for false coincidences at the arrival times of 5.0–5.8 μs. The coincidence events within these windows were counted during 120 s at each photon energy in the range of about 287–293.5 eV, using an energy step of 20 meV; the total measuring time was above 16 h. The results are shown in Fig. 4 after subtraction of false coincidences and normalization to the photon flux. The yield of H(HR)-CH_n^+ coincidences has been scaled at the C $1s \rightarrow 3pt_2$ excitation to the same height as the total ion yield (TIY) that was measured simultaneously. The relative heights of the two H(HR)-photoion coincidence yields reflect the experimental observations.

We see that metastable H(HR) atoms are produced at every C $1s \rightarrow$ Rydberg excitation. In comparison to the TIY, their production is slightly enhanced at the 4p and 4d resonances, and increasingly more at higher Rydberg ($n \geqslant 5$) excitations before forming maxima just above the C 1s IP. The H(HR)-CH_n^+ coincidence yield reveals two clear peaks and a hint of a shoulder above the ionization limit, whereas the corresponding

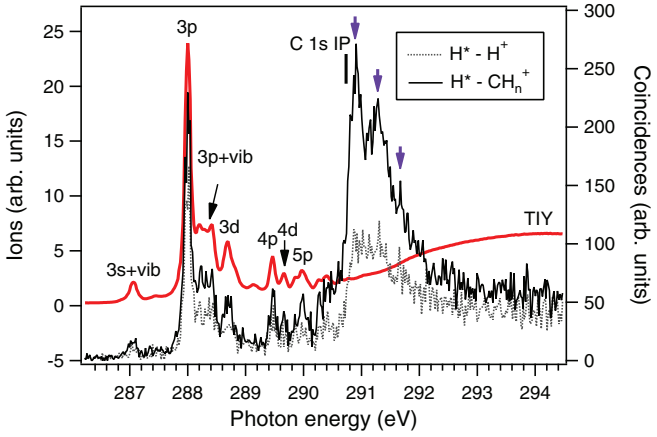

FIG. 4. (Color online) The H*-H^+ and H*-CH_n^+ coincidence yields at the C 1s edge in comparison with the TIY. The C 1s excitations have been assigned according to [15,29]. Photon energy resolution was about 70 meV. The arrows above the C 1s IP (290.735 eV [29]) indicate the photon energies at which the coincidence spectra of Fig. 5 were measured.

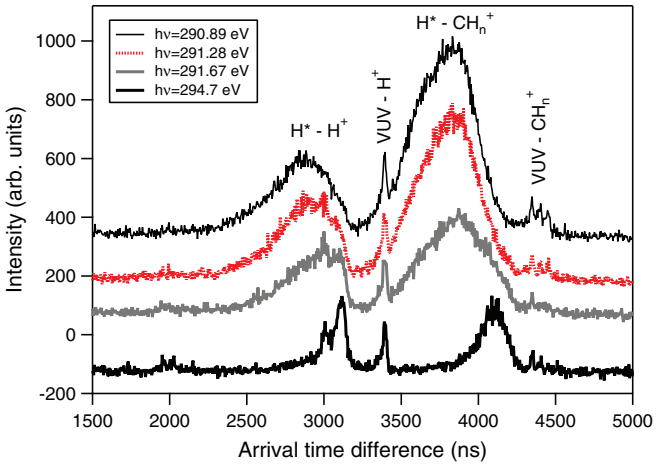

FIG. 5. (Color online) Four neutral-particle–photoion coincidence spectra measured at the C 1*s* edge. The three lowest photon energies correspond to those indicated by arrows in Fig. 4; the measuring time was 4 h for each of them. The bottom spectrum was measured about 4 eV above the C 1*s* IP for 2 h, but the exit slit of the monochromator was twice larger. The spectra have been shifted vertically for clarity.

features are less evident in the H(HR)-H^+ coincidence yield. We ascribe the peaks to the C $1s^{-1}$, $\upsilon = 0$ and 1 states, i.e., to the vibrational structure of the core-ionized state. The energy separation between the peaks agrees well with the difference of about 397 meV observed between the $\upsilon = 0$ and 1 vibrational levels of the C $1s^{-1}$ state using photoelectron spectroscopy [34,35]. In our experiment, the maxima occur at higher excitation energy than the nominal C 1*s* thresholds because of PCI. The resulting recapture processes yield molecular ions in 2h-1e states whose dissociation in turn produces excited H atoms.

Neutral-particle–photoion coincidence spectra were measured at the two maxima and at the shoulder observed in the H(HR)-CH_n^+ coincidence yield just above the C 1s threshold (these photon energies are indicated by arrows in Fig. 4) and additionally about 4 eV above the C 1*s* IP. The results are shown in Fig. 5 after scaling of the 294.7 eV spectrum (it was multiplied by 1.3) so that the heights of the VUV-photon–H^+ coincidence peaks are similar. The H(HR)-photoion coincidence peaks are much more intense and much wider in the three "threshold" spectra than in the spectrum measured at the higher photon energy. There are no resonances or ionization limits in the excitation energy range between the C 1*s* IP and 295 eV [34]. Thus the huge differences in the spectra should be attributed to recapture processes that occur in just-above-threshold photoionization, but hardly at all at the photon energy of 294.7 eV. The shift of the H(HR)-photoion coincidence intensity towards longer arrival time differences indicates that considerably slower H(HR) atoms are ejected from the molecular ions just at the threshold than at photon energies when recapture events are not important (see also Fig. 4). Some H(HR)-CH_n^+ coincidence intensity extends below the VUV-H^+ peak, which means that the coincidence yields shown in Fig. 4 underestimate the importance of these processes at the C 1*s* threshold.

Our experiments show that the H(HR)-CH_n^+ coincidence channel is more enhanced at the C 1*s* threshold than the H(HR)-H^+ channel. As the relative intensities of the H(HR)-photoion coincidence channels are similar around the photon energy of 294.7 eV (Fig. 5), recapture processes appear to favor the creation of H(HR) atoms together with CH_n^+ ions rather than with H^+ ions. The dissociation after recapture is determined by the double valence-hole configuration, like after normal Auger decay, because the interaction between the electron in a faraway Rydberg orbital and the valence electrons is weak. The normal Auger decay populates the final states $2a_1^{-2}$, $2a_1^{-1}1t_2^{-1}$, and $1t_2^{-2}$, among which the last mentioned are by far the most intense (see e.g., [15,24]). The fragmentation of CH_4^{2+} after Auger decay has been studied using coincidence techniques, for instance, by Kukk *et al.* [24] and by Flammini *et al.* [25]. From the analysis of the Auger electron-ion-ion coincidence maps the latter authors concluded that the fragmentation process is stepwise and mainly occurs via the formation and dissociation of the CH_3^+ intermediate.

In the special case of core ionization just above the C 1*s* threshold, we expect to observe H^*-H^+ coincidences only when the fragmentation of CH_4^{2+} yields two H^+ ions, one of which becomes a metastable neutral atom by receiving the recaptured photoelectron upon dissociation. Auger electron-H^+–H^+ coincidences were not reported in [25], but quite a few of them were actually observed when the kinetic energy of the Auger electrons was set at 231, 238, and 250 eV (±1.1%) [36], corresponding to the $2a_1^{-2}$, $2a_1^{-1}1t_2^{-1}$, and $1t_2^{-2}$ final states, respectively. It was not possible to quantify the relative intensities of the Auger electron-H^+–H^+ coincidences, as some protons were lost because of their large momenta in the direction perpendicular to the axis of the ion TOF spectrometer used in [25]. However, we believe that the branching ratio of the Auger electron–H^+–H^+ coincidences to all Auger electron-ion-ion coincidences decreases with the increase of the Auger electron kinetic energy. The relative intensities of the Auger electron-CH_n^+ ($n = 0$–3) coincidences were in fact highest for the Auger electron kinetic energy of 250 eV [25], corresponding to the $1t_2^{-2}$ final states. As the $1t_2^{-2}$ states of CH_4^{2+} cannot undergo second-step Auger decay, it is unlikely that their dissociation produces two H^+ ions together with a CH_n^+ ($n = 0$–3) fragment; that is possible only if a H^- ion is also created.

The lowest limit to produce two protons from CH_4 via the reaction $CH_4 \rightarrow CH_2 + H^+ + H^+$ is 36.5 eV [37]. In the recent work of Wolff *et al.* [16], dissociation channels associated with two protons were observed to be important already at the first studied photon energy, 40 eV. The branching ratio of the H^+-H^+ ion pair is the most intense one among all possible ion pairs in the photon energy range of 100–480 eV [16]. Interestingly, it shows a distinct drop at the C 1*s* edge, while the branching ratios of the H^+-CH_n^+ ($n = 1$–3) ion pairs are enhanced at that photon energy.

In summary, the yields of both H(HR)-CH_n^+ ($n = 0$–3) and H(HR)-H^+ coincidence channels are greatly enhanced at the C 1*s* threshold due to recapture processes. The increase in the former channel is stronger. Following C 1*s* photoionization, normal Auger decay mostly populates the $1t_2^{-2}$ final states, whose dissociation yields particularly many molecular ions CH_n^+ ($n = 1$–3) [25]. The C 1*s* photoelectron may be recaptured during Auger decay and it may end up in a

HR orbital of any fragment after dissociation. If the recapture probability does not depend on the character of the Auger final states, the relative intensities of the Auger transitions and subsequent dissociation channels can explain why the production of H(HR)-CH_n^+ ($n = 0$–3) pairs is larger than that of the H(HR)-H^+ pairs in C 1s threshold photoionization.

We observe that the coincidence spectrum measured at the photon energy of 291.67 eV has already changed from the one taken at 290.98 eV (see Fig. 5): The relative intensity of the H(HR)-CH_n^+ coincidence feature has dropped and the H(HR)-photoion coincidence intensity has partially shifted towards the corresponding VUV-photon–photoion coincidence peaks. In order to explain these changes, we should remember that at the photon energy of 291.67 eV core photoionization can take place from three vibrational levels ($\upsilon = 0$–2) of the C $1s^{-1}$ state. In the coincidence spectrum, we measure the sum of their contributions. At $h\nu = 291.67$ eV, the photoelectron recapture occurs efficiently if the photoelectron comes from the C $1s^{-1}$, $\upsilon = 2$ state. Instead, it appears that if the photoelectron comes from the C $1s^{-1}$, $\upsilon = 0$ state, its recapture has become significantly less probable. The resulting H*-photoion coincidence intensity starts to show characters that are associated with above-threshold C 1s ionization, represented by the lowermost spectrum in Fig. 5.

D. Effect of the electric field

The detected events in our spectra can be interpreted qualitatively as VUV-photon–photoion and metastable-atom–photoion coincidences, as we have presented above. We can, however, gain more insight into the atomic states contributing to the spectra if we consider the effect of the electric field. In principle, all excited H atoms have enough internal energy to be detected by the MCP detector, hence their detection as metastable atoms is just a matter of lifetime. The electric field can change the lifetimes of the excited states or it can ionize them [38].

In our experimental configuration the detected metastable atoms should have a lifetime of at least ∼300 ns, which is the time difference between the VUV-photon–H^+ and the H^*-H^+ coincidence peaks in Figs. 2 and 3. The H(2s) state is metastable and it has enough internal energy (10.20 eV) to be detected by an MCP detector. However, an electric field F of ∼320 V/cm normally applied in the interaction region can cause a mixing between the $2s_{1/2}$ and $2p_{1/2}$ states and efficiently deplete the H(2s) population via Lyman-α emission [39]. According to Ref. [40], the lifetime of the H(2s) state is about 8 ns in the field conditions used in the interaction region. That lifetime is compatible with the observed FWHM (25 ns) of the VUV-photon–H^+ coincidence peak in Fig. 2. So instead of giving rise to the H^*-photoion coincidences, the H(2s) state is expected to contribute to the VUV-photon–photoion coincidences. The radiative lifetimes of the H(nl) states with $nl = 5s, 12p, 9d$, and $7f$ exceed 300 ns in field-free conditions [23]; the lifetime increases with n for a given l. In the presence of the electric field (the Stark effect), the wave functions and the energy levels of the hydrogen atom can be described by the principal quantum number n, the magnetic quantum number m, and parabolic quantum numbers n_1 and n_2, which are related by $n_1 + n_2 + |m| = n - 1$ (see, e.g., [30,41]). The radiative transition probabilities depend on the new quantum numbers, but the total decay probability from a given shell n remains the same as in the field-free case [42]. Calculations [30] indicate that in the electric field the average lifetime of a couple hundred nanoseconds is reached for $n = 7$. We therefore assume that the metastable fragments observed in our experiments were H($n \geqslant 7$) atoms.

A constant dc field can also ionize H(HR) atoms. The electric field required to field ionize H(n) atoms at the rate of $\sim 10^9$ s^{-1}, in a very rough approximation, ranges from $\sim 5.1 \times 10^9/(9n^4)$ V/cm to $\sim 5.1 \times 10^9/(4n^4)$ V/cm for, respectively, the lowest energy and highest energy members of the n Stark manifold [38]. Using the first relation, we estimated that H(HR) atoms with $n \geqslant 37$ were field ionized in the interaction region in the usual measuring conditions (see Fig. 1). However, the resulting ions were pushed towards the ion TOF spectrometer and did not give any start signals. The field was lower, about 180 V/cm, between the repeller mesh and the second mesh in front of the neutral-particle MCP and was not expected to field ionize further H(HR) atoms. In contrast, F was much higher, ∼5.3 kV/cm, between the second mesh and the front of the neutral-particle detector, so it could ionize H(HR) atoms with $n \geqslant 18$. These atoms were converted to H^+ ions, which were then accelerated towards the MCP detector and detected. It should be remembered that all the given ranges of n are approximate.

In order to verify whether field ionization played a role in our experiments, we performed two coincidence measurements in which the potential of the second mesh was changed from +300 V to −1.8 kV (see Fig. 1). In that way, the region of the highest field (now ∼2.8 kV/cm) was shifted further away from the MCP detector. That field could ionize H($n \geqslant 21$) atoms at the rate of $\sim 10^9$ s^{-1}. The coincidence spectra measured at the photon energy of 290.89 eV in the two different conditions of electric fields are presented in Fig. 6. This photon energy is just above the C 1s IP and corresponds to the energy where the H(HR)-CH_n^+ ($n = 0$–3)

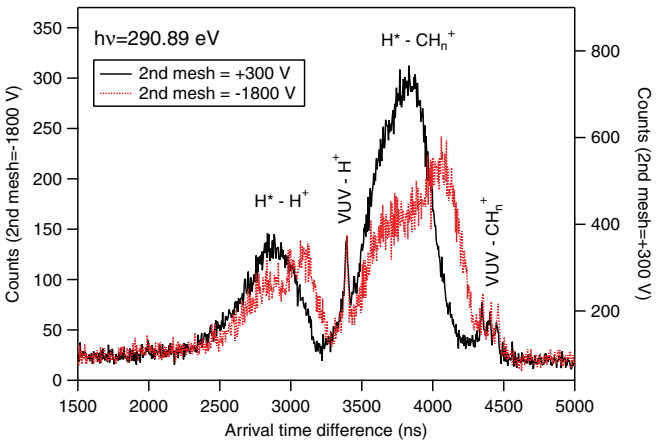

FIG. 6. (Color online) The neutral-particle–photoion coincidence spectrum of methane measured at the photon energy of 290.89 eV with two different sets of electric fields. The spectrum taken with the second mesh set at −1800 V was measured for 2 h, and the other spectrum for 4 h. The shift of the H^*-photoion coincidence peaks proves that the electric field ionizes H atoms in high Rydberg states.

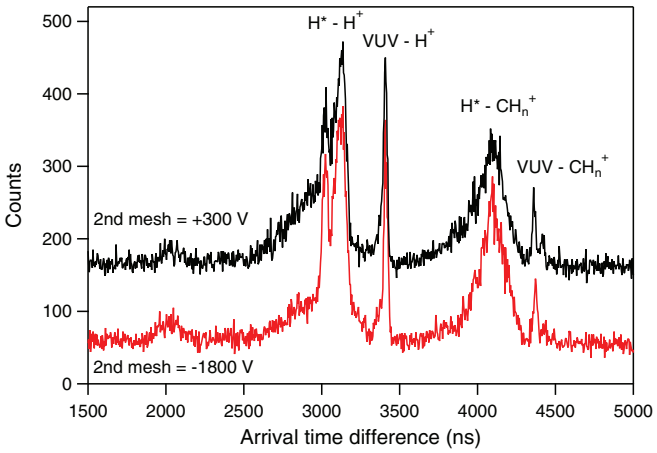

FIG. 7. (Color online) The neutral-particle–photoion coincidence spectrum of methane measured at the photon energy of 334 eV with two different sets of electric fields. The sharp peak at 3000 ns and the bump around 2000 ns are due to electron-triggered start signals. The top spectrum has been shifted upwards by 100 counts for clarity.

coincidence yield reached the maximum (see Fig. 4). The "metastable" features clearly moved with the change of the field, indicating that field ionization converts some H(HR) atoms to H^+ ions. Subsequent acceleration of the H^+ ions made them arrive sooner in the detector. Therefore, the closer to the corresponding VUV-photon–photoion coincidence peaks the H(HR)-photoion coincidence events appeared, the further away from the detector were the metastable atoms field ionized. This measurement proves that photoionization of CH_4 at the photon energy just above the C 1s IP led to creation of H(HR) atoms with $n \geqslant 21$ or so. Even though these particles were detected as ions in the neutral-particle detector, they were created as metastable atoms in the interaction region.

A coincidence experiment with two different electric field settings was also performed at the photon energy of 334 eV. The spectra, shown in Fig. 7, are characterized by the relative intensity increase of the H^*-photoion coincidence features as compared to the measurement done at the C $1s \rightarrow 3p$ resonance (Fig. 2). The changes of the spectral features that occurred upon the change of the electric field were much smaller than at the C 1s threshold (Fig. 6), but they do exist. The right edge of the H^*-H^+ coincidence peak remained at the same position with respect to the VUV-photon–H^+ coincidence peak. The left flank of the feature became weaker and shifted slightly towards the right, which may be due to field ionization of H(HR) atoms with $n \geqslant 21$ and the subsequent acceleration of the created H^+ ions. The changes were even smaller in the H^*-$CH_n{}^+$ coincidence peak.

The photon energy of 334 eV, which was used in the spectra of Fig. 7, exceeds the C 1s shake-up photoionization thresholds [34]. The removal of a C 1s electron can therefore be accompanied by a simultaneous excitation of a valence electron to unoccupied Rydberg orbitals, whereby excitations to the two lowest orbitals, $3sa_1$ and $3pt_2$, are the most probable [34]. Fluorescence experiments in CH_4 indicate that C 1s shake-up ionization leads to an intensity increase in Balmer-α and Lyman-α emission [43]. Balmer-α emission produces metastable H(2s) atoms through H(3p)→H(2s) transitions but, as was discussed above, the H(2s) states should be depopulated fast by fluorescence, made possible by the mixing of the $2s_{1/2}$ and $2p_{1/2}$ states in the electric field. Instead, we tentatively attribute the part of the H^*-H^+ coincidence structure that did not move with the change of the electric field (in the arrival time differences of ∼3000–3200 ns) to H(n) atoms with $n \approx 7$–20. Correspondingly, the part of the H^*-H^+ coincidence structure that moved with the change of F can be attributed to H(n) atoms with $n \approx 21$–36, whereas H(HR) atoms with $n \geqslant 37$ can be field ionized in the interaction region and should not contribute to the spectrum (as before, the given ranges of n are approximate). H(HR) atoms should be minority dissociation fragments at the photon energy of 334 eV, which is above resonances and shake-up satellite thresholds and even above core-valence double-ionization thresholds [44].

E. Kinetic energy distribution of H* atoms

Using the VUV-H^+ coincidence peak as a time reference, we can obtain information about the kinetic energies of metastable H(HR) atoms that are ejected in dissociation together with a H^+ ion. It takes about 80 ps for (VUV) photons to pass from the interaction region to the two sections of the MCP that were used in coincidence measurements. This time is so short that it can be neglected in present considerations. The lifetime of excited states of H atoms depends on the quantum numbers of the electron orbital in the electric field. To eliminate at least partly the contribution of the lifetime, we set the zero of the flight time of H(HR) atoms to be at the half height on the right flank of the VUV-H^+ coincidence peak (i.e., at the rising edge in time). We assume that neutral H^* atoms reached the detector in the measurements performed at the C $1s \rightarrow 3pt_2$ and $3dt_2$ Rydberg resonances (i.e., they were not ionized by the dc field), because the observed H(HR)-H^+ coincidence feature was quite similar to the one recorded at the photon energy of 334 eV, which did not react strongly to the change of the electric field (see Figs. 2, 3, and 7). In contrast, we suppose that field ionization took place at the second mesh in the measurement performed at the photon energy of 290.89 eV, which is just above the C 1s IP. After field ionization, the H^+ were quickly accelerated to high velocities in the electric field between the second mesh and the MCP detector (see Fig. 1). It can be easily calculated that these particles remained neutral for the major part of their flight times; for instance, this fraction is 98.7% for a H(HR) atom with the initial kinetic energy of 10 eV. This factor was approximately accounted for by neglecting the flight time as ionized species and by elongating the flight distance as neutral by 1% for all kinetic energies. Finally, we also assume that the start signals were detected at the points of the MCP that corresponded to the average flight path length. In this way, we can convert the time scale of the measured spectra to the kinetic energy scale of the H(HR) atoms. Figure 8 shows the number of H(HR)-H^+ coincidences within 0.5-eV-wide windows that were obtained from the sum of the measurements performed at the C $1s \rightarrow 3pt_2$, $3pt_2 + \nu_1$, and $3dt_2$ excitations (see spectra in Figs. 2 and 3) as well as from the spectrum measured at the photon energy of 290.89 eV (Fig. 5). Because of the many assumptions made, these kinetic energy distributions are only approximate, especially for fast H^* atoms.

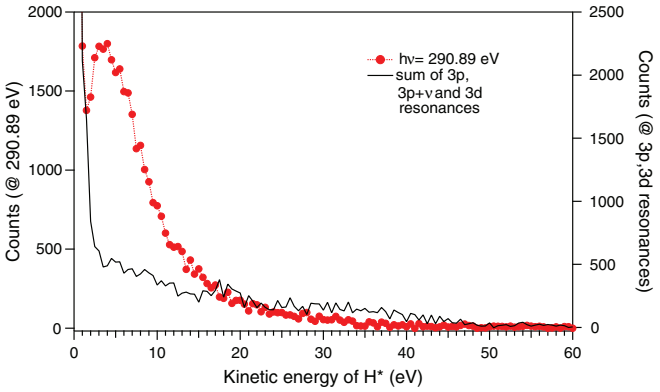

FIG. 8. (Color online) The approximate kinetic energy distributions of H* atoms at the C 1s threshold ($h\nu = 290.89$ eV, filled circles connected by a dotted line) and at the C $1s \rightarrow 3pt_2$, $3pt_2 + \nu_1$, and $3dt_2$ resonances (solid curve).

Both curves in Fig. 8 display high intensity at energies just above zero (the transformed kinetic energy scale of the H* atoms begins at about 0.25 eV). The height of that peak depends on the choice of the background level; we set it at the average count number in the region above 4700 ns in the coincidence spectra (i.e., above all the coincidence peaks). In the measurement done at the C 1s threshold (filled circles connected by a dotted line in Fig. 8), the kinetic energy distribution of metastable H* atoms displays another feature, which is centered at ~3.5 eV kinetic energy, and a slowly decaying intensity up to 35 or 40 eV. Proportionally less metastable H* atoms with kinetic energies between 2 and 15 eV are created at the C $1s \rightarrow 3pt_2$, $3pt_2 + \upsilon_1$, and $3dt_2$ excitations than at the C 1s threshold. (The feature appearing around 19 eV in the resonant measurements is not real, but it results from the electron contamination in start signals.) The clear peak observed in the time-of-flight spectra around 3100 ns (see Figs. 2 and 3) is transformed to a low and wide feature between 24 and 45 eV kinetic energy.

We next consider how the feature around 3.5 eV kinetic energy could form after photoionization at 290.89 eV photon energy. Let us recall that recapture processes take place at this photon energy. After Auger decay, the final state is doubly charged and starts to dissociate because of Coulombic forces (the $CH_4{}^{2+}$ ion is not stable). If the photoelectron is recaptured, one of the fragments becomes neutral, and the Coulombic push ends before the two fragments have fully separated. If this mechanism is valid, the kinetic energy of the metastable H atom formed after recapture should be smaller than the kinetic energy of H^+ after dissociation without recapture processes. Flammini *et al.* [25] determined the kinetic energies of H^+ ions from Auger electron-ion-ion coincidence maps: their values range from 4.08(±0.83) eV to 7.19(±1.20) eV depending on the dissociation channel and the kinetic energy of the Auger electron. These results are in qualitative agreement with the maximum at 3.5 eV in Fig. 8. Some metastable H atoms are, however, clearly faster than the H^+ ions detected in the study of Flammini *et al.* [25]. The difference could be due to other dissociation channels that are associated with higher kinetic energy releases. In particular, recapture processes occurring in the context of double Auger decay [44] can be envisioned to provide a stronger Coulombic kick to a departing H* atom, because the molecular ion after such decay is $CH_4{}^{3+}$ (two Auger electrons are emitted simultaneously). We in fact expect that dissociation produces more likely two H^+ ions after double Auger decay than after normal Auger decay; the creation of the H^+-H^+ ion pair is a requirement for the emergence of the H^+-H* pair after recapture. Therefore, double Auger decay likely produces more H^+-H* coincidences than what is its probability among all Auger decay channels.

The kinetic energies of the order of 30 eV found for H* atoms at the C $1s \rightarrow 3p$ and $3d$ resonances are very high. We expect the highest kinetic energies for the lightest fragment if dissociation is sequential. As was mentioned above, sequential dissociation was found to be the main dissociation mechanism after normal Auger decay [25]. After resonant Auger decay, the final state ion $CH_4{}^+$ would first dissociate to $CH_3{}^+ + H^*$, whereby H* receives most of the available kinetic energy. For instance, if E_{kin} of H* is 30 eV, that of $CH_3{}^+$ would be 2 eV. In the second step, $CH_3{}^+$ would need dissociate to H^+ and CH_2 (or to the constituents of the latter fragment) so that H(HR)-H^+ coincidences can be observed. The dissociation energy of $CH_4 \rightarrow H + H^+ + CH_2$ is 22.80 eV [45]. Taking into account also the internal energy of the excited H atom—it is close to 13.6 eV for high Rydberg states—we estimate that the final states after resonant Auger decay should have above 68 eV binding energy so that a H(HR) atom can appear with $E_{kin} = 30$ eV. This binding energy is higher than that of any major features in the resonant Auger spectrum measured at the C $1s \rightarrow 3pt_2$ excitation [26], with only very weak intensity in the appropriate binding energy region, which corresponds to very highly excited states of $CH_4{}^+$. It is also possible, and perhaps even more likely, that such fast H(HR) atoms originate from dissociation after resonant double Auger decay, i.e., when the core-excited state decays by emitting two electrons simultaneously. Most metastable H* atoms are, however, considerably slower. A similar consideration for H* atoms having the kinetic energy of 5 eV is that they can originate from final states with the binding energy of ~42 eV or higher. There is considerable intensity in the relevant part of the resonant Auger spectrum [26]. In the case of relatively slow H* atoms, it is also possible that the molecular ion (after resonant Auger decay) dissociates in one step only, e.g., $CH_4^+ \rightarrow H^* + H^+ + CH_2$.

IV. CONCLUSIONS

We have studied photofragmentation of the methane molecule at the C 1s threshold by observing coincidences between neutral metastable particles and photoions as well as coincidences between VUV photons and photoions. Two metastable fragment-photoion coincidence features were observed: one of them originating from H*-H^+ coincidences, the other from H*-$CH_n{}^+$ ($n = 0$–3) coincidences. Metastable H atoms observed were in so highly excited Rydberg states that their lifetime is of the same order or larger than their flight time in our experiment (⩾300 ns). VUV photons triggering the coincidence events are mostly due to Lyman emission in excited H atoms that are created when the final states of (resonant) Auger decay dissociate. The intensity ratios between the H*-photoion and VUV-photon–photoion

coincidence peaks are very similar in the spectra measured at the C $1s \rightarrow 3pt_2$ and $3dt_2$ resonances. This observation can be explained by the l mixing of the H(nl) states in the presence of the electric field. For the same reason, we did not observe metastable H($2s$) atoms, but the metastable atom signal was likely due to H(n) atoms with $n \geqslant 7$. At the C $1s \rightarrow 3pt_2$ and $3dt_2$ resonances, the kinetic energy distribution of H^* atoms displayed a slowly decaying curve, which extended even up to 40 eV. So fast fragments could be explained by sequential dissociation—in which $CH_4{}^+$ ions produced in resonant Auger decay first dissociate into $CH_3^+ + H^*$, followed by the dissociation of the molecular fragment ion—or by double Auger decay.

Metastable H atom production was strongly enhanced just above the C $1s$ threshold. The H^*-$CH_n{}^+(n = 0–3)$ coincidence yield displayed two clear maxima above the C $1s$ IP. Their energy difference corresponds to the vibrational energy of the symmetric stretching in the C $1s^{-1}$ state of $CH_4{}^+$. Thus we observed metastable atom production from vibrationally resolved core-ionized states. The increase of metastable fragment production at the C $1s$ threshold was attributed to recapture processes. The slow photoelectron is pushed back to the molecular ion after emission of an Auger electron, whereby $CH_4{}^+$ ions in highly excited states are created. When these molecular ions dissociate, excited H atoms with an electron in a high Rydberg orbital are created. A simple change of potentials in the experiment revealed the presence of H(n) atoms with $n \geqslant 21$ at the C $1s$ threshold. The kinetic energy distribution of the H^* atoms, which was derived from the coincidence spectrum measured at the C $1s$ threshold, shows a structure that extends from 2 eV to above 30 eV, with a maximum around 3.5 eV. Metastable-fragment–photoion coincidence spectroscopy can offer a fruitful method to study the post-collision interaction and recapture processes in molecules.

ACKNOWLEDGMENTS

We are grateful to R. Flammini for communicating his unpublished results to us and to the staff of Elettra–Sincrotrone Trieste for assistance during the experiments.

[1] Y. Hikosaka, P. Lablanquie, and E. Shigemasa, J. Phys. B **38**, 3597 (2005).
[2] Y. Hikosaka, T. Kaneyasu, and E. Shigemasa, J. Korean Phys. Soc. **53**, 3798 (2008).
[3] J. R. Harries, T. Gejo, K. Honma, M. Kuniwake, J. P. Sullivan, M. Lebech, and Y. Azuma, J. Phys. B **44**, 095101 (2011).
[4] T. Gejo, T. Tamura, K. Honma, E. Shigemasa, Y. Hikosaka, and Y. Tamenori, J. Chem. Phys. **136**, 054201 (2012).
[5] Y. Hikosaka, T. Gejo, T. Tamura, K. Honma, Y. Tamenori, and E. Shigemasa, J. Phys. B **40**, 2091 (2007).
[6] A. Marquette, M. Gisselbrecht, W. Benten, and M. Meyer, Phys. Rev. A **62**, 022513 (2000).
[7] A. Kivimäki, G. Vall-llosera, M. Coreno, M. A. Huels, M. Stankiewicz, and E. Rachlew, J. Phys. B **42**, 185103 (2009).
[8] E. Melero García, A. Kivimäki, L. G. M. Pettersson, J. Álvarez Ruiz, M. Coreno, M. de Simone, R. Richter, and K. C. Prince, Phys. Rev. Lett. **96**, 063003 (2006).
[9] K. Jakubowska, G. Vall-llosera, A. Kivimäki, M. Coreno, E. Melero García, M. Stankiewicz, and E. Rachlew, J. Phys. B **40**, 1489 (2007).
[10] A. Kivimäki, J. Álvarez-Ruiz, T. J. Wasowicz, C. Callegari, M. de Simone, M. Alagia, R. Richter, and M. Coreno, J. Phys. B **44**, 165103 (2011).
[11] A. Kivimäki, M. Coreno, R. Richter, J. Álvarez Ruiz, E. Melero García, M. de Simone, V. Feyer, G. Vall-llosera, and K. C. Prince, J. Phys. B **39**, 1101 (2006).
[12] J. W. Au, G. Cooper, G. R. Burton, T. N. Olney, and C. E. Brion, Chem. Phys. **173**, 209 (1993).
[13] N. N. Matsuzawa, A. Ishitani, D. A. Dixon, and T. Uda, J. Phys. Chem. A **105**, 4953 (2001).
[14] J. Schirmer, A. B. Trofimov, K. J. Randall, J. Feldhaus, A. M. Bradshaw, Y. Ma, C. T. Chen, and F. Sette, Phys. Rev. A **47**, 1136 (1993).
[15] K. Ueda, M. Okunishi, H. Chiba, Y. Shimizu, K. Ohmori, Y. Sato, E. Shigemasa, and N. Kosugi, Chem. Phys. Lett. **236**, 311 (1995).
[16] W. Wolff, L. Sigaud, E. C. Montenegro, V. L. B. de Jesus, R. L. Cavasso Folho, S. Pilling, and A. C. F. Santos, J. Phys. Chem. A **117**, 56 (2013).
[17] K. Furuya, K. Ishikawa, and T. Ogawa, Chem. Phys. Lett. **319**, 335 (2000).
[18] H. Fukuzawa, T. Odagiri, T. Nakazato, M. Murata, H. Miyagi, and N. Kouchi, J. Phys. B **38**, 565 (2005).
[19] K. C. Prince *et al.*, J. Synchrotron Rad. **5**, 565 (1998).
[20] M. Barat, J. C. Brenot, J. A. Fayeton, and Y. J. Picard, Rev. Sci. Instrum. **71**, 2050 (2000).
[21] M. Tronc, G. C. King, R. C. Bradford, and F. H. Read, J. Phys. B **9**, L555 (1976).
[22] ACAM Messelectronic GmBH, www.acam.de.
[23] Ya. F. Verolainen and A. Ya. Nikolaich, Sov. Phys. Usp. **25**, 431 (1982).
[24] E. Kukk *et al.*, J. Phys. B **40**, 3677 (2007).
[25] R. Flammini, M. Satta, E. Fainelli, G. Alberti, F. Maracci, and L. Avaldi, New J. Phys. **11**, 083006 (2009).
[26] A. Kivimäki, M. Neeb, B. Kempgens, H. M. Köppe, and A. M. Bradshaw, J. Phys. B **29**, 2701 (1996).
[27] T. A. Field and J. H. D. Eland, J. Electron Spectrosc. Relat. Phenom. **73**, 209 (1995).
[28] H. A. Bethe and E. E. Salpeter, *Quantum Mechanics of One- and Two-Electron Systems* (Plenum, New York, 1977).
[29] M. de Simone, M. Coreno, M. Alagia, R. Richter, and K. C. Prince, J. Phys. B **35**, 61 (2002).
[30] K. Omidvar, At. Data Nucl. Data Tables **28**, 215 (1983).
[31] M. Carlsson Göthe, B. Wannberg, L. Karlsson, S. Svensson, P. Baltzer, F. T. Chau, and M.-Y. Adam, J. Chem. Phys. **94**, 2536 (1991).
[32] K. Kuramoto, M. Ehara, and H. Nakatsuji, J. Chem. Phys. **122**, 014304 (2005).
[33] B. L. Peko and T. M. Stephen, Nucl. Instrum. Methods Phys. Res., Sect. B **171**, 597 (2000).
[34] H. M. Köppe, B. S. Itchkawitz, A. L. D. Kilcoyne, J. Feldhaus, B. Kempgens, A. Kivimäki, M. Neeb, and A. M. Bradshaw, Phys. Rev. A **53**, 4120 (1996).

[35] T. X. Carroll, N. Berrah, J. Bozek, J. Hahne, E. Kukk, L. J. Sæthre, and T. D. Thomas, Phys. Rev. A **59**, 3386 (1999).
[36] R. Flammini (private communication).
[37] G. Dujardin, D. Winkoun, and S. Leach, Phys. Rev. A **31**, 3027 (1985).
[38] W. A. Chupka, J. Chem. Phys. **98**, 4520 (1993).
[39] W. D. Fite, R. T. Brackmann, D. G. Hummer, and R. F. Stebbings, Phys. Rev. **116**, 363 (1959).
[40] V. I. Radchenko and G. D. Ved'manov, J. Exp. Theor. Phys. **80**, 670 (1995).
[41] V. S. Lisitsa, Sov. Phys. Usp. **30**, 927 (1988).
[42] D. R. Herrick, Phys. Rev. A **12**, 1949 (1975).
[43] M. Coreno, A. Kivimäki, M. de Simone, E. Melero García, G. Vall-llosera, J. Álvarez Ruiz, E. Rachlew, and M. Stankiewicz, Phys. Scr. **76**, C90 (2007).
[44] J. H. D. Eland, P. Linusson, L. Hedin, E. Andersson, J.-E. Rubensson, and R. Feifel, Chem. Phys. Lett. **485**, 21 (2010).
[45] J. A. R. Samson, G. N. Haddad, T. Masuoka, P. N. Pareek, and D. A. L. Kilcoyne, J. Chem. Phys. **90**, 6925 (1989).